



Estimates of micro-, nano-, and picoplankton contributions to particle export in the northeast Pacific

B. L. Mackinson¹, S. B. Moran¹, M. W. Lomas², G. M. Stewart³, and R. P. Kelly¹

¹Graduate School of Oceanography, University of Rhode Island, Narragansett, RI 02882, USA

²Bigelow Laboratory for Ocean Sciences, East Boothbay, ME 04544, USA

³Queens College and Graduate Center, City University of New York, Queens, NY 11367, USA

Correspondence to: B. L. Mackinson (bmackinson@my.uri.edu)

Received: 23 July 2014 – Published in Biogeosciences Discuss.: 27 August 2014

Revised: 8 April 2015 – Accepted: 18 April 2015 – Published: 5 June 2015

Abstract. The contributions of micro-, nano-, and picoplankton to particle export were estimated from measurements of size-fractionated particulate ²³⁴Th, organic carbon, and phytoplankton indicator pigments obtained during five cruises between 2010 and 2012 along Line P in the subarctic northeast Pacific Ocean. Sinking fluxes of particulate organic carbon (POC) and indicator pigments were calculated from ²³⁴Th–²³⁸U disequilibria and, during two cruises, measured by a sediment trap at Ocean Station Papa. POC fluxes at 100 m ranged from 0.65 to 7.95 mmol m⁻² d⁻¹, similar in magnitude to previous results at Line P. Microplankton pigments dominate indicator pigment fluxes (averaging 69 ± 19 % of total pigment flux), while nanoplankton pigments comprised the majority of pigment standing stocks (averaging 64 ± 23 % of total pigment standing stocks). Indicator pigment loss rates (the ratio of pigment export flux to pigment standing stocks) point to preferential export of larger microplankton relative to smaller nano- and picoplankton. However, indicator pigments do not quantitatively trace particle export resulting from zooplankton grazing, which may be an important pathway for the export of small phytoplankton. These results have important implications for understanding the magnitude and mechanisms controlling the biological pump at Line P in particular, and more generally in oligotrophic gyres and high-nutrient, low-chlorophyll (HNLC) regions where small phytoplankton represent a major component of the autotrophic community.

1 Introduction

Phytoplankton community structure exerts an important influence on the strength and efficiency of the biological pump (Michaels and Silver, 1988; Boyd and Newton, 1999; Thibault et al., 1999; Brew et al., 2009; Lomas and Moran, 2011). Small nano- and picoplankton dominate the phytoplankton community in the oligotrophic gyres and high-nutrient, low-chlorophyll (HNLC) oceanographic regions. It has traditionally been thought that small phytoplankton represent a relatively small fraction of the downward flux of particulate organic carbon (POC) (see Table 1 for definitions of abbreviations) relative to larger phytoplankton, such as diatoms, which are generally thought to contribute disproportionately to POC export (e.g., Michaels and Silver, 1988). Recent studies have challenged this idea, suggesting that small phytoplankton contribute significantly to POC export, possibly through aggregation and incorporation into fecal pellets (Richardson and Jackson, 2007; Amacher et al., 2009; Stukel and Landry, 2010; Lomas and Moran, 2011; Stukel et al., 2013). A better understanding of the controls on the relative importance of small phytoplankton in POC export is needed to refine our understanding of the magnitude and mechanisms controlling the biological pump, particularly as recent climate models predict an expansion of the oligotrophic gyres where small cells dominate (Irwin et al., 2006; Polovina et al., 2008; Morán et al., 2010).

Ocean Station Papa (OSP, 50° N, 145° W), the site of one of the longest-running ocean time series, is located in the northeast Pacific Ocean in one of three major HNLC regions. Previous attempts to resolve the apparent paradox

Table 1. Summary of abbreviations used.

Term	Abbreviation	Unit
Net primary production	NPP	$\text{mmol m}^{-2} \text{d}^{-1}$
Suspended particulate organic carbon	POC	$\mu\text{mol L}^{-1}$
^{234}Th activity	^{234}Th	dpm L^{-1}
^{238}U activity	^{238}U	dpm L^{-1}
Chlorophyll <i>a</i> concentration	Chl <i>a</i>	ng L^{-1}
Fucoxanthin concentration	FUCO	ng L^{-1}
Peridinin concentration	PER	ng L^{-1}
19'-hexanoyloxyfucoxanthin concentration	HEX	ng L^{-1}
19'-butanoyloxyfucoxanthin concentration	BUT	ng L^{-1}
Alloxanthin concentration	ALLO	ng L^{-1}
Total chlorophyll <i>b</i> concentration	TChl <i>b</i>	ng L^{-1}
Zeaxanthin concentration	ZEA	ng L^{-1}
Microplankton proportion factor	mPF	
Nanoplankton proportion factor	nPF	
Picoplankton proportion factor	pPF	
^{234}Th flux	F_{Th}	$\text{dpm m}^{-2} \text{d}^{-1}$
^{234}Th -derived POC flux	F_{POC}	$\text{mmol m}^{-2} \text{d}^{-1}$
^{234}Th -derived <i>e</i> ratio ($F_{\text{POC}} / \text{NPP}$)	ThE ratio	
Sediment trap ^{234}Th flux	F_{Th}	$\text{dpm m}^{-2} \text{d}^{-1}$
Sediment trap POC flux	F_{POC}	$\text{mmol m}^{-2} \text{d}^{-1}$
^{234}Th -derived pigment flux	F_{pigment}	$\text{mg m}^{-2} \text{d}^{-1}$
Sediment trap pigment flux	F_{pigment}	$\text{mg m}^{-2} \text{d}^{-1}$

of low phytoplankton biomass and high nitrate concentrations at OSP concluded that a bottom-up control related to iron limitation is most important for large phytoplankton (Muggli et al., 1996; Harrison, 2006; Marchetti et al., 2006), while microzooplankton grazing exerts a strong top-down control on pico- and nanoplankton (Landry et al., 1993; Harrison et al., 1999; Rivkin et al., 1999). Primary production at the stations proximal to the coast on Line P (P4 and P12) is not iron-limited, and diatom blooms are typically observed in spring and late summer (Boyd and Harrison, 1999; Thibault et al., 1999). At the offshore stations (including OSP), the phytoplankton community is dominated by cells $< 5 \mu\text{m}$ and the seasonal variability of primary production is relatively low (~ 25 in winter and $\sim 67 \text{ mmol C m}^{-2} \text{d}^{-1}$ in summer) (Boyd and Harrison, 1999; Thibault et al., 1999; Choi et al., 2014). In contrast to the low variability in primary production, POC export recorded by moored sediment traps at OSP exhibits a stronger seasonal cycle with fluxes at 200 m depth ranging from $\sim 0.4 \text{ mmol C m}^{-2} \text{d}^{-1}$ in winter to $\sim 2.4 \text{ mmol C m}^{-2} \text{d}^{-1}$ in summer (Timothy et al., 2013). The average annual sediment trap POC flux at OSP ($1.4 \pm 1.1 \text{ mmol C m}^{-2} \text{d}^{-1}$) is nearly 5 times lower than the annual net community production (ANCP) at OSP ($6.3 \pm 1.6 \text{ mmol C m}^{-2} \text{d}^{-1}$), suggesting that the majority of organic carbon export is due to active transport by zooplankton and/or dissolved organic carbon (DOC) export (Timothy et al., 2013; Emerson, 2014).

This study builds upon prior investigations of phytoplankton community composition and export production along Line P by examining the distributions of organic carbon, phytoplankton indicator pigments, and ^{234}Th in three particle size-fractions. Sinking fluxes of POC and indicator pigments from the upper waters ($\sim 100 \text{ m}$) were calculated from the ^{234}Th – ^{238}U disequilibrium and, during two cruises, measured at OSP using free-floating sediment traps. A comparison of indicator pigment fluxes with the respective standing stocks suggests that microplankton (20–200 μm) make up a higher percentage of particle export than biomass, whereas pico- and nanoplankton (0.2–2 μm and 2–20 μm) make up a lower percentage of particle export than biomass.

2 Methods

2.1 Study location

Sample collection was conducted at five stations along Line P (P4, P12, P16, P20, and P26 (OSP)) during cruises aboard the CCGS *John P. Tully* in August 2010, February 2011, June 2011, February 2012, and June 2012 (Fig. 1, Table 2). Line P is located at the southern edge of the Alaskan Gyre, and the prevailing winds and surface currents are west–east (Bograd et al., 1999). Because precipitation and continental runoff exceed evaporation, a permanent halocline exists at $\sim 100 \text{ m}$ impeding deep winter mixing. In addition, a seasonal ther-

Table 2. Cruise dates and sample collection along Line P. Stations where total ^{234}Th (Total Th), particulate thorium (Part. Th), water column pigments (WC Pig), particulate pigments (Part. Pig), and sediment trap (Traps) were sampled are indicated.

Cruise dates	P4	P12	P16	P20	P26
Aug 2010 (19–31 Aug 2010)	Total Th	Total Th WC Pig	Total Th WC Pig	Total Th WC Pig	Total Th
Feb 2011 (9–15 Feb 2011)		Total Th WC Pig	Total Th WC Pig	Total Th WC Pig	Total Th
Jun 2011 (4–16 Jun 2011)	Total Th WC Pig	Total Th WC Pig	Total Th WC Pig	Total Th WC Pig	Total Th Part. Th WC Pig Part. Pig Traps
Feb 2012 (7–19 Feb 2012)	Total Th Part. Th WC Pig Part. Pig	Total Th Part. Th WC Pig Part. Pig	Total Th Part. Th WC Pig Part. Pig	Total Th Part. Th WC Pig Part. Pig	Total Th Part. Th WC Pig Part. Pig
Jun 2012 (23 May–7 Jun 2012)	Total Th Part. Th WC Pig Part. Pig	Total Th Part. Th WC Pig Part. Pig	Total Th Part. Th WC Pig Part. Pig	Total Th Part. Th WC Pig Part. Pig	Total Th Part. Th Part. Pig Traps

moocline forms at ~ 50 m in spring and shoals to ~ 20 m in summer (Freeland et al., 1997; Thibault et al., 1999; Freeland, 2013; Timothy et al., 2013).

2.2 Net primary production by ^{14}C incubation

Rates of net primary production (NPP) were determined following the protocols outlined in Lomas et al. (2012). Samples were collected with Niskin bottles from seven depths in the euphotic zone corresponding to 1, 5, 9, 17, 33, 55, and 100 % of surface irradiance. Three “light” bottles, a single “dark” bottle, and a single initial (T_0) bottle were each spiked with $\sim 10 \mu\text{Ci NaH}^{14}\text{CO}_3$. A sub-sample to confirm total added activity was removed from the T_0 bottle at each light depth and immediately added to an equal volume of β -phenylethylamine. Bottles were incubated under simulated in situ conditions, using neutral density screening to mimic light levels at the depth of sample collection, in an on-deck incubator for ~ 24 h. After incubation, 125 mL of sub-samples from each light and dark bottle was filtered through an Ahlstrom 151 ($0.7 \mu\text{m}$ nominal pore size) and a Whatman Track Etch $5 \mu\text{m}$ filter and rinsed with 10 % HCl. Samples were counted on a Perkin Elmer TriCarb 2900LR ~ 48 h after the addition of 5 mL of Ultima Gold (Perkin Elmer, USA) scintillation cocktail.

2.3 Water column ^{234}Th

Total ^{234}Th (dissolved and particulate) analysis followed the procedures outlined in Bauman et al. (2013). Briefly, samples (4 L) were collected by Niskin bottle at 12 depths (surface to ~ 500 m) and spiked with ^{230}Th to monitor Th recovery. Samples were then treated with 7–8 drops of concentrated NH_4OH solution, followed by $25 \mu\text{L}$ of 0.2 M KMnO_4 , and finally with $11.5 \mu\text{L}$ of 1.0 M MnCl_2 to form a MnO_2 precipitate that quantitatively scavenges Th (Benitez-Nelson et al., 2001; Buesseler et al., 2001; van der Loeff et al., 2006). After 1 h, samples were vacuum filtered onto 25 mm glass microfiber filters (GMF, $1 \mu\text{m}$ nominal pore size) that were frozen for later analysis in the shore-based laboratory. To prepare samples for counting, filters were dried at 50°C for ~ 24 h, mounted on acrylic planchets, and covered with aluminum foil. To quantify ^{234}Th , the beta emission of $^{234\text{m}}\text{Pa}$ ($E_{\text{max}} = 2.19 \text{ MeV}$; $t_{1/2} = 1.2 \text{ min}$) was counted using a Risø National Laboratory low-background beta detector (Roskilde, Denmark). Each sample was counted four times over a period of approximately six half-lives, with the first count made at least 10 days after collection to allow for the decay of short-lived isotopes, and the final count used to quantify background levels. Data were fitted to the ^{234}Th decay curve to calculate the decay-corrected activity at the time of sample collection. Following the ^{234}Th analysis, Th was radiochemically purified and ^{230}Th was measured by alpha particle emission in order to determine scavenging efficiency. Small-volume scavenging efficiencies were found

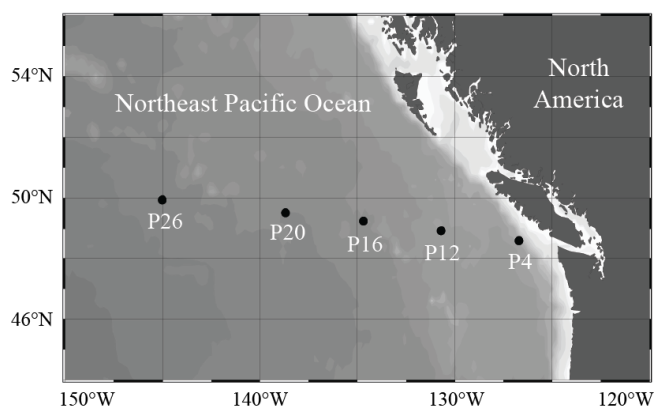


Figure 1. Map showing the Line P stations sampled in this study.

to be $> 90\%$. ^{238}U activities were calculated from salinity using the relationship $^{238}\text{U} = 0.07081 \times S$ (‰) (Chen et al., 1986).

2.4 Water column POC, Chl *a*, and indicator pigments

Water samples for POC, Chl *a*, and phytoplankton indicator pigments were collected from the same depths in the photic zone as for NPP samples. Suspended POC was measured on 1 L seawater samples filtered onto pre-combusted Ahlstrom 151 filters and frozen at -20°C until analysis. Samples were dried at 60°C in a drying oven, fumed in a desiccator containing concentrated hydrochloric acid for 24 h to remove inorganic carbonates, and dried again at 60°C . Samples were then analyzed on an EA-440 Analyzer (Exeter Analytical, Inc., Chelmsford, MA). Chl *a* samples were analyzed using the methods outlined in Lomas et al. (2012). Separate samples ($\sim 0.2\text{ L}$) were filtered onto Ahlstrom 151 and $5\ \mu\text{m}$ Whatman Track Etch polycarbonate filters and frozen at -20°C until analysis. Samples were then extracted in 5 mL of 90 % acetone for 24 h at -20°C and analyzed using a calibrated TD-700 fluorometer.

Indicator pigment samples were collected on separate Ahlstrom 151 filters and stored at -80°C until analysis by high-performance liquid chromatography (HPLC) at the Bermuda Institute of Ocean Sciences in the Bermuda Atlantic Time-series Study (BATS) laboratory (Knap et al., 1997). Fucoxanthin (FUCO), peridinin (PER), 19'-hexanoyloxyfucoxanthin (HEX), 19'-butanoyloxyfucoxanthin (BUT), alloxanthin (ALLO), total chlorophyll *b* (TChl *b*), and zeaxanthin (ZEA) were analyzed as indicator pigments based on their correspondence to particular phytoplankton taxonomic groups. Indicator pigment proportion factors (PFs) were calculated to further analyze the size distribution of the phytoplankton community (Hooker et al., 2005; Lomas and Moran, 2011). The sum of FUCO and PER concentrations was used to determine the microplankton proportion factor (mPF), while the sum of HEX, BUT, ALLO, and TChl *b* was used to determine the

nanoplankton proportion factor (nPF), and ZEA was used to determine the picoplankton proportion factor (pPF) (Hooker et al., 2005; Lomas and Moran, 2011). Hooker et al. (2005) included TChl *b* in pPF, but because *Prochlorococcus* is not found in the study region, it was assumed in this study that any Chl *b* would be found in cells (e.g., chlorophytes and euglenophytes) in the nanoplankton size class.

2.5 In situ pump sampling

Large-volume in situ pumps (Challenger Oceanic Systems and Services, UK; McLane Scientific, Falmouth, MA) were deployed for approximately 4 h at depths of 30, 50, 100, 150, and 200 m. Each pump sampled 100–1000 L to collect size-fractionated particles, with seawater passing sequentially through 53, 10, and $1\ \mu\text{m}$ Nitex screens. Particles were resuspended by ultrasonication in $0.7\ \mu\text{m}$ pre-filtered seawater and filtered onto separate pre-combusted GF/F filters for parallel analysis. Indicator pigment samples were stored at -80°C until analysis by high-performance liquid chromatography (HPLC) at the Bermuda Institute of Ocean Sciences in the BATS laboratory (Knap et al., 1997). Filters for analysis of POC and ^{234}Th were frozen at -20°C until analysis. A sub-sample ($\sim 30\%$ by weight) was cut with acetone-cleaned stainless steel scissors from each ^{234}Th filter for POC analysis, and these sub-samples were dried and fumed with concentrated HCl as described above. POC was then measured using a CE 440 CHN Elemental Analyzer (Exeter Analytical, Inc., Chelmsford, MA). The ^{234}Th filter subsample was dried at 60°C in a drying oven and counted on a Risø beta detector as noted above.

2.6 Sediment trap sampling

Surface-tethered particle interceptor traps (PITS) with cylindrical tubes (KC Denmark, Silkeborg, Denmark) were deployed for ~ 3 days at station P26 during the June 2011 and June 2012 cruises to collect particles at the depths of 30, 50, 100, 150, and 200 m. Due to time constraints during the cruises, it was not possible to deploy sediment traps at any other stations sampled as part of this study. The trap design and sampling procedure is described in Baumann et al. (2012). Four tubes (72 mm diameter, 450 mm length) were used at each depth, and tubes were filled with non-poisoned, $0.4\ \mu\text{m}$ filtered brine ($S = \sim 85\%$) prior to deployment. Upon recovery trap brines were combined, particles were resuspended and filtered onto pre-combusted GF/F filters, and “swimmers” were removed. Filters were stored frozen and later analyzed for POC, ^{234}Th , and indicator pigments as described above.

Table 3. Total net primary production (NPP) and $> 5 \mu\text{m}$ size-fractionated NPP determined from simulated in situ incubations. ^{234}Th -derived POC flux (P_{POC}) and sediment trap POC flux (F_{POC}) determined at the base of the photic zone and the corresponding ThE ratios ($P_{\text{POC}} / \text{NPP}$) and trap e ratios ($F_{\text{POC}} / \text{NPP}$). Stations P26-D and P26-R refer to sediment trap deployment and recover stations, respectively.

Cruise	Station	Integration depth (m)	Total NPP ($\text{mmol m}^{-2} \text{d}^{-1}$)	$> 5 \mu\text{m}$ NPP ($\text{mmol m}^{-2} \text{d}^{-1}$)	P_{POC} ($\text{mmol m}^{-2} \text{d}^{-1}$)	F_{POC} ($\text{mmol m}^{-2} \text{d}^{-1}$)	ThE ratio	Trap e ratio
Feb 2011	P20	77	36.64	3.26				
Jun 2011	P26-D	83	105.14	13.67	2.94	5.91	0.03	0.06
	P26-R	85	78.75	12.98	2.75	5.91	0.03	0.08
Feb 2012	P4	50	27.91	3.58	7.29		0.26	
	P12	95	34.56	4.58	4.65		0.13	
	P26	75	23.41	5.22	0.31		0.01	
Jun 2012	P4	103	82.36	39.55	7.95		0.10	
	P12	164	40.24	4.16	2.12		0.05	
	P20	115	57.84	4.10	0.54		0.01	
	P26	60	49.45	9.28	2.96	6.55	0.06	0.13

3 Results

3.1 Hydrography and NPP

Depth sections of temperature and density anomaly (σ_t) were generated using results from all CTD casts for a given cruise to improve horizontal data resolution (Fig. 2). The seasonal change in water temperature is largely confined to the upper ~ 100 m. Surface temperatures in August 2010 were $\sim 14^\circ\text{C}$, while during the February cruises, surface temperatures were slightly cooler offshore ($\sim 6^\circ\text{C}$) than inshore ($\sim 8^\circ\text{C}$). During the June cruises, inshore temperatures were warmer (~ 10 – 12°C) while offshore temperatures remained relatively cool ($\sim 8^\circ\text{C}$). Density anomaly did not vary greatly between cruises below ~ 100 m. During the winter, a pool of less dense water (1023 – 1025 kg m^{-3}) was observed toward the coast (east of $\sim 126^\circ\text{W}$). During the June cruises, this pool was observed extending west to $\sim 130^\circ\text{W}$ and during August 2010, it extended out to OSP (145°W). These data follow the expected seasonal pattern of a well-mixed water column in winter and increasing stratification moving from spring to summer.

Total NPP and $> 5 \mu\text{m}$ size-fractionated NPP values were trapezoidally integrated over the euphotic zone (Table 3). A maximum total NPP of $91.9 \text{ mmol m}^{-2} \text{d}^{-1}$ was measured at station P26 during June 2011, whereas the lowest value of $23.4 \text{ mmol m}^{-2} \text{d}^{-1}$ was measured at station P26 during February 2012. These values agree to within a factor of 2 with the seasonal averages reported by Boyd and Harrison (1999). A maximum $> 5 \mu\text{m}$ NPP of $39.6 \text{ mmol m}^{-2} \text{d}^{-1}$ was at station P4 during June 2012 and a minimum of $3.2 \text{ mmol m}^{-2} \text{d}^{-1}$ was measured at station P20 in February 2011.

3.2 Small- and large-volume POC concentrations

Suspended POC concentrations from Niskin bottle samples collected in the photic zone range from 1.1 to $7.1 \mu\text{mol L}^{-1}$. POC concentrations were generally lowest at the base of the photic zone, though decreasing concentrations with depth were not observed at all stations (Table S1 in Supplement). The highest suspended POC concentrations were measured at station P4 during all cruises. POC concentrations were also measured in three size fractions of particles collected with large-volume in situ pumps (Table S2). Concentrations of each size fraction tended to decrease with depth and were typically less than $0.5 \mu\text{mol L}^{-1}$ at all depths. One exception was at station P26 during February 2011 when POC concentrations at 30 m were between 1.8 and $2.9 \mu\text{mol L}^{-1}$ for all size fractions.

The concentrations of POC collected using small-volume and large-volume methods often do not agree for samples collected at the same location and depth (Gardner, 1977; Moran et al., 1999; Liu et al., 2005, 2009). As reported in these previous studies, POC concentrations measured by large-volume in situ pumps (summed for all size fractions) are significantly (ANOVA, $p < 0.05$) less than small-volume POC measurements from the same station and similar depth (Fig. 3a). Explanations put forth to account for this discrepancy include DOC adsorption to filters, pressure effects on particle retention in pump samples, the collection of zooplankton by Niskin bottles but not pumps, and particle washout from pump filters (Moran et al., 1999; Liu et al., 2005, 2009). In this study, the smallest pump size fraction was collected using a $1 \mu\text{m}$ Nitex screen, not a GF/F, resulting in the pumps missing the portion of the POC on particles between 0.7 and $1 \mu\text{m}$, which may further contribute to the difference observed between the two methods. Lomas and Moran (2011) reported that sonication of in situ pump

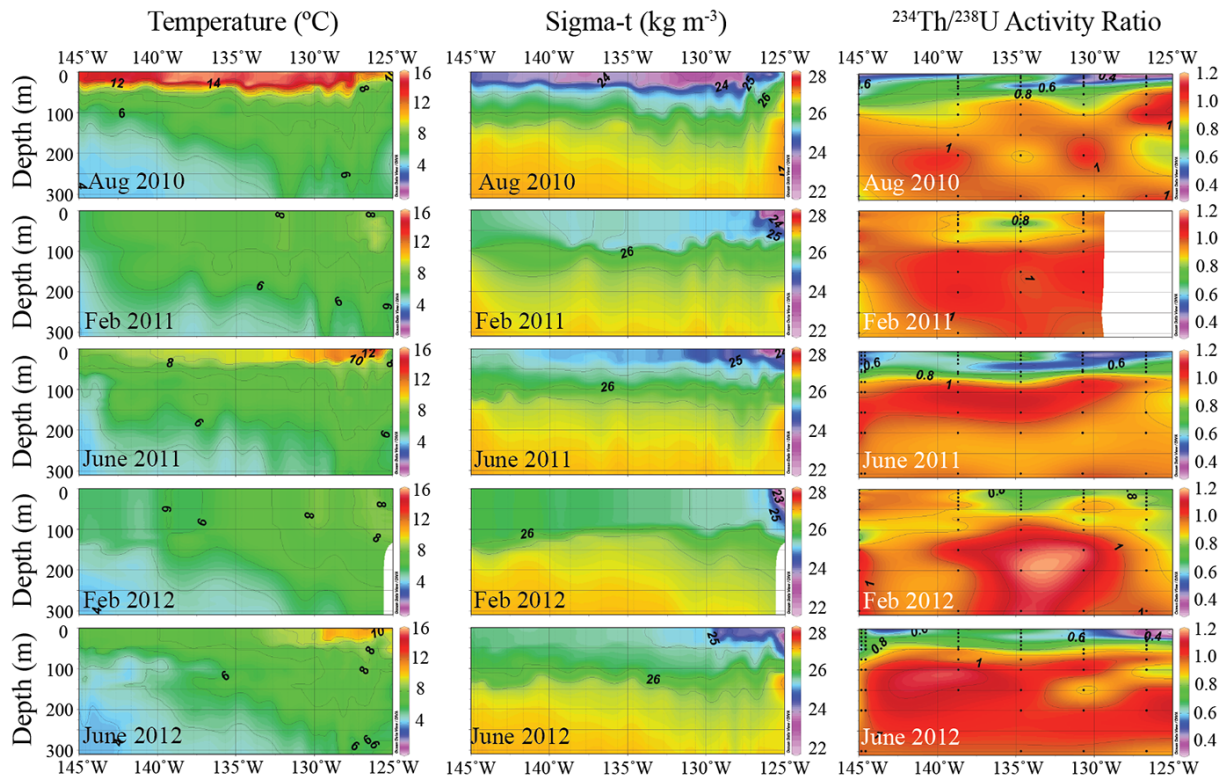


Figure 2. Temperature ($^{\circ}\text{C}$), σ_T (kg m^{-3}), and $^{234}\text{Th}/^{238}\text{U}$ activity ratio distributions along Line P cruises in August 2010, February 2011, June 2011, February 2012, and June 2012.

samples to resuspend particles from the Nitex screens had no significant effect on measured POC concentrations.

3.3 Particulate ^{234}Th and POC / ^{234}Th ratios

Size-fractionated particulate ^{234}Th activities in samples collected using an in situ pump generally decrease with depth, and are typically less than 0.1 dpm L^{-1} (Table S2). As with in situ pump POC concentrations, station P26 during February 2011 is an exception, with values exceeding 0.1 dpm L^{-1} for all size fractions at 30 m and throughout most of the water column for the 1–10 μm fraction. Size-fractionated POC / ^{234}Th ratios (Fig. 4a, Table S2) are less than $\sim 6 \mu\text{mol dpm}^{-1}$ for all size classes at most stations, with higher values measured at stations P4 and P12 in February 2012 and P4 in June 2012. POC / ^{234}Th ratios tend to decrease or remain constant with depth, with one exception at station P12 during February 2012 where the maximum POC / ^{234}Th was at 100 m for all size fractions. Also, the POC / ^{234}Th ratio does not vary greatly between size fractions (Fig. 4a), as was observed in Speicher et al. (2006) and Brew et al. (2009).

The accuracy of ^{234}Th as a tracer of POC export depends on the assumption that ^{234}Th and POC are sinking on the same particles, and therefore sinking at the same rate (Moran et al., 2003; Smith et al., 2006; Speicher et al., 2006; Burd et

al., 2007; Brew et al., 2009). A high degree of correlation between the size-fractionated distributions of ^{234}Th and POC (Fig. 4b–d) along Line P provides evidence in support of this assumption. All correlations were statistically significant ($p < 0.05$) and imply a strong coupling between particulate ^{234}Th and POC for all cruises. In addition, the clustering of data for the different size fractions of particles (Fig. 4) indicates that in February 2012 the 10–53 μm size class contained the highest percentage of POC and particulate ^{234}Th , while the $> 53 \mu\text{m}$ size class contained the lowest percentage. In June 2012, the 1–10 μm size class had the lowest percentage of POC and particulate ^{234}Th , while both the 10–53 μm and the $> 53 \mu\text{m}$ fractions contained higher percentages (Fig. 4b–d).

3.4 Small-volume Chl *a* and indicator pigments

Concentrations of total Chl *a* and $> 5 \mu\text{m}$ Chl *a* measured by fluorometer (Table S1) were trapezoidally integrated over the photic zone to determine respective standing stocks. During August 2010, the $> 5 \mu\text{m}$ fraction accounted for $> 30\%$ of the Chl *a* at all stations, with a maximum of 50% at station P26. During the other four cruises, the $> 5 \mu\text{m}$ size fraction generally accounted for $< 30\%$ of the total Chl *a*, except at station P26 in February 2012 and station P4 in June 2012. Previous studies have reported that larger cells

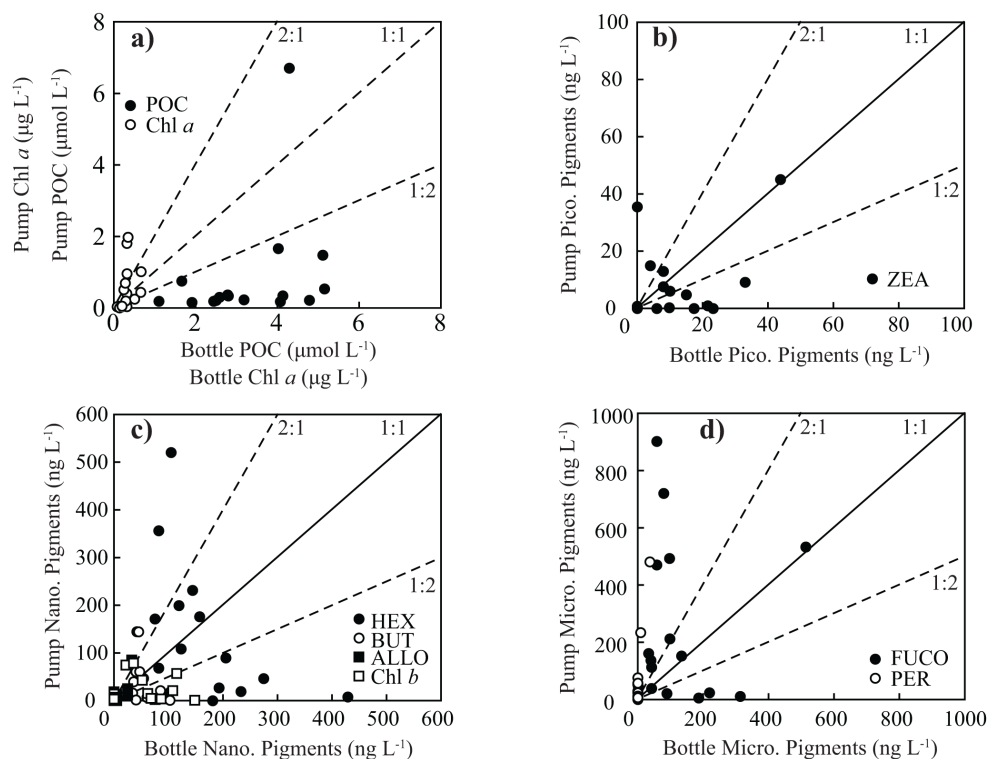


Figure 3. Comparison of small-volume Niskin bottle and large-volume in situ pump measurements of (a) POC, (b) picoplankton indicator pigments, (c) nanoplankton indicator pigments, and (d) microplankton pigments. Niskin bottle measurements are lower than pump measurements for microplankton pigments, and higher for nanoplankton pigments and POC.

are more abundant at stations closer to the coast (Boyd and Harrison, 1999), though this was not always apparent. The highest $> 5 \mu\text{m}$ percentage of Chl *a* was measured at station P26 during August 2010, June 2011, and February 2012. Phytoplankton indicator pigments and Chl *a* concentrations in samples from the euphotic zone samples were also measured by HPLC (Table S1). HPLC and fluorescence Chl *a* concentrations generally agreed to within a factor of 2, and the correlation between the two measurements was statistically significant ($p < 0.05$) (Fig. S1 in the Supplement). The correlation between the sum of the indicator pigment concentrations and the Chl *a* concentration was statistically significant ($p < 0.05$) and roughly 1 : 1, suggesting that the indicator pigments examined in this analysis accounted for most of the phytoplankton biomass (Fig. S2). Furthermore, the correlation between the $> 5 \mu\text{m}$ fraction of Chl *a* and mPF is statistically significant ($p < 0.05$), suggesting that this PF is a reasonable representation of that size fraction of the phytoplankton community. Profiles of indicator pigment concentrations were trapezoidally integrated over the photic zone to quantify standing stocks (Table 4). FUCO was the most abundant microplankton pigment, and HEX was the most abundant nanoplankton pigment at most stations. Indicator pigment PFs (Fig. 5, Table S3) reveal that the phytoplankton community was typically dominated by nanoplankton,

although at P4, and to a lesser extent at P20 in June 2012, microplankton pigments made up the bulk of the sample (~ 86 and $\sim 52\%$, respectively).

3.5 Large-volume size-fractionated Chl *a* and indicator pigments

Size-fractionated Chl *a* and indicator pigment concentrations were also measured using an in situ pump (Table S4). Chl *a* was once again strongly correlated in a roughly 1 : 1 ratio with the sum of the indicator pigments ($p < 0.05$) (Fig. S3). The highest Chl *a* concentrations were measured in the 10–53 μm fraction during all cruises. In February 2012, the $> 53 \mu\text{m}$ fraction generally had the lowest concentrations, while in June 2012 and June 2011 the lowest concentrations were generally in the 1–10 μm fraction.

Ideally, small-volume and large-volume concentrations of Chl *a* and indicator pigments should agree for samples collected at the same station and depth, but this was not observed in this study (Fig. 3). Although differences between small- and large-volume measurements of POC have been reported (Gardner, 1977; Moran et al., 1999; Liu et al., 2005, 2009), few studies have compared Niskin bottle and in situ pump measurements of indicator pigments (Lomas and Moran, 2011). Relative to bottle samples, the pump samples indicate higher concentrations of microplankton pigments FUCO and

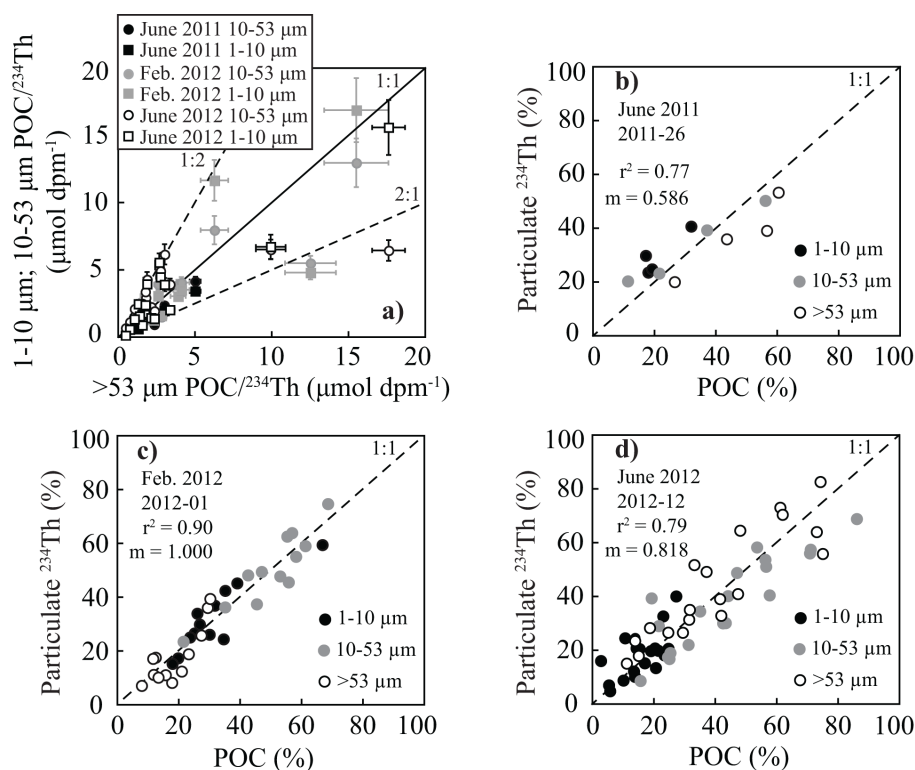


Figure 4. (a) POC / ^{234}Th ratios on 1–10 μm particles and on 10–53 μm particles plotted against the POC / ^{234}Th ratio on > 53 μm particles. Fractional distributions of POC and particulate ^{234}Th are plotted for three size classes of particles. The percentage of total POC associated with each size class is plotted against the percentage of total particulate ^{234}Th for samples collected at stations on Line P during (b) June 2011, (c) February 2012, and (d) June 2012. The correlation coefficient (r^2) and the slope of the linear regression (m) are shown for each cruise.

PER and lower concentrations of ZEA and TChl *b*, which are pigments associated with pico- and nanoplankton (Fig. 3b–d). Large-volume pump and small-volume bottle measurements of the nanoplankton indicator pigments HEX, BUT, and ALLO generally agree within a factor of 2 (Fig. 3b–d). Given the small size of ZEA-containing *Synechococcus* and TChl *b*-containing chlorophytes and prasinophytes, it is likely that many of these cells pass through the 1 μm Nitex screen which would lead to under-sampling by the pumps (Liu et al., 2005). Bottles may under-sample large, rare cells because the small volume might not be a statistically representative sample (Lomas and Moran, 2011). Furthermore, larger cells may settle below the spigot of the Niskin bottles, leading to a further bias against the collection of large cells (Gardner, 1977; Gundersen et al., 2001). Pumps sample higher concentrations of Chl *a* than bottles (Fig. 3a) at stations with high concentrations of Chl *a*, but when Chl *a* concentrations are low ($< 200 \text{ ng L}^{-1}$), the pumps tend to under-sample relative to the bottles.

Given these sampling differences, it is important to note that although the total concentrations (summed for all size fractions) measured by the in situ pumps may be inaccurate, it is still possible that the > 53 μm fraction accurately represents the composition of sinking particles. The disruption

of loosely bound aggregates during collection by the pumps could cause an error in the > 53 μm fraction, but this is considered unlikely due to the presence of nanoplankton (and in some cases picoplankton) pigments in this fraction. Furthermore, a recent study in the Sargasso Sea employed a similar methodology and also found picoplankton pigments in three particle size classes, each > 10 μm (Lomas and Moran, 2011).

Indicator pigment PFs calculated for the size-fractionated particles (Table S3) and plotted against depth (Figs. 6–8) reveal that while the overall indicator pigment concentrations vary with depth and across size fractions, the PFs do not exhibit a systematic pattern of variation across size classes, depths, or seasons. The picoplankton pigment ZEA typically represents < 10% of the total indicator pigments for all size classes. Microplankton pigments dominated samples at station P4 in February 2012 and June 2012, with mPFs typically exceeding 0.5 and 0.8, respectively. In addition, mPFs were high at station P26 during these times, with values generally exceeding 0.5 (Figs. 7–8). Nanoplankton pigments dominated at station P12 in February 2012 cruise with nPFs exceeding 0.5 for most samples. As with the small volume samples, FUCO was usually the most abundant mi-

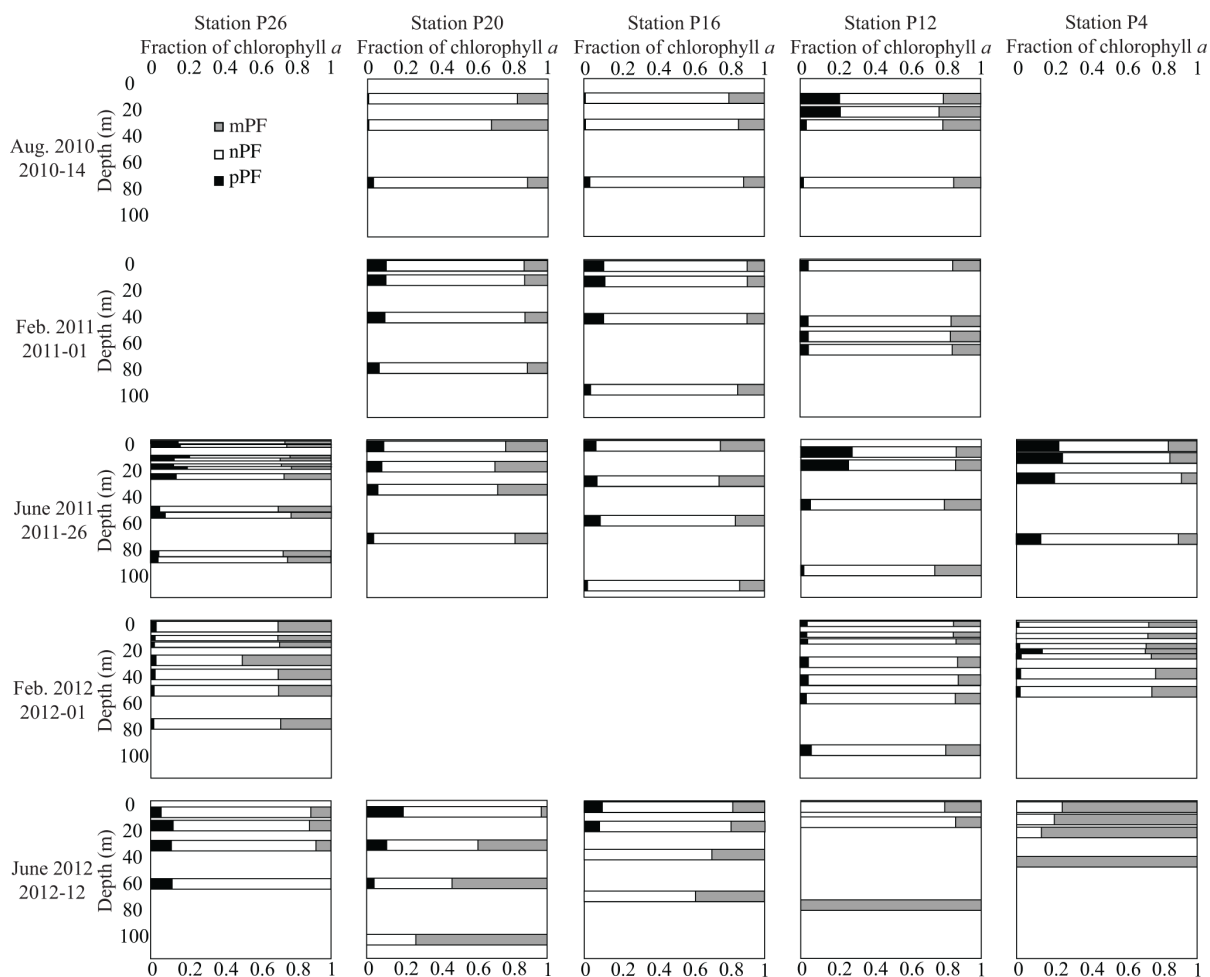


Figure 5. Pigment proportion factors (PFs) for each phytoplankton size class plotted as a function of sample depth at stations sampled on Line P during the five cruises in the study. All data were collected from Niskin bottles.

croplankton pigment while HEX was usually the most abundant nanoplankton pigment (Table S4).

3.6 Total ^{234}Th , $^{234}\text{Th}/^{238}\text{U}$ activity ratios, and ^{234}Th fluxes

Total (dissolved + particulate) ^{234}Th activities, ^{238}U activities, and $^{234}\text{Th}/^{238}\text{U}$ activity ratios are listed in Table S5. Depth sections of these $^{234}\text{Th}/^{238}\text{U}$ activity ratios (Fig. 2d) indicate that areas of low $^{234}\text{Th}/^{238}\text{U}$ are prevalent in spring and summer and corresponding to periods known to have high particle export in this region (Wong et al., 1999; Timothy et al., 2013). ^{234}Th fluxes (P_{Th}) were calculated using these $^{234}\text{Th}/^{238}\text{U}$ results and a 2-D steady-state model of the radiochemical balance for ^{234}Th in the upper ocean,

$$\frac{\partial A_{\text{Th}}}{\partial t} = A_{\text{U}}\lambda_{\text{Th}} - A_{\text{Th}}\lambda_{\text{Th}} - P_{\text{Th}} + K_{\text{h}} \frac{\partial^2 A_{\text{Th}}}{\partial z^2} + U_{\text{h}} \frac{\partial A_{\text{Th}}}{\partial x}, \quad (1)$$

where A_{U} is the activity of ^{238}U , λ_{Th} is the ^{234}Th decay constant, A_{Th} is the activity of ^{234}Th , P_{Th} is the vertical

flux of ^{234}Th on sinking particles, K_{h} is the eddy diffusion coefficient, and U_{h} is the current velocity (Coale and Bruland, 1985; Charette et al., 1999). Assuming a steady state ($\partial A_{\text{Th}}/\partial t = 0$) over several weeks to months, and that the diffusive flux of ^{234}Th is small relative to advection and can therefore be ignored, the vertical flux of ^{234}Th (in $\text{dpm m}^{-2} \text{d}^{-1}$) is defined by

$$P_{\text{Th}} = \int_0^z \left[\lambda_{\text{Th}}(A_{\text{U}} - A_{\text{Th}}) + U_{\text{h}} \frac{\partial A_{\text{Th}}}{\partial x} \right] dz, \quad (2)$$

where z is the depth of the water column over which the flux is measured. In this study, the gradient of thorium ($\partial A_{\text{Th}}/\partial x$) was only measured in the east–west direction (along Line P). Therefore, x is the east–west distance across which the gradient will be measured and U_{h} is the east–west current velocity. Current velocities determined from 5-year seasonal averages of surface drifter data (available from Fisheries and Oceans Canada) were found to be 6 ± 4 for the February

Table 4. Chl *a* and indicator pigment standing stocks determined by integrating small volume pigment concentrations (determined by HPLC) across the photic zone, pigment fluxes (^{234}Th - and PITS-derived) measured at the base of the photic zone, and pigment loss rates, or the percent of the surface concentration represented by those fluxes. Pigment standing stocks are in mg m^{-2} and pigment fluxes are in $\text{mg m}^{-2} \text{d}^{-1}$.

Cruise	Station	Depth	Chl <i>a</i>	FUCO	PER	HEX	BUT	ALLO	Chl <i>b</i>	ZEA
Aug 2010 (2010–2014)	P12	Surface (1–75 m)	23.918	3.498	0.375	7.705	1.165	0.220	4.038	1.435
	P16	Surface (1–75 m)	14.165	1.288	0.340	6.010	1.018	0.065	2.588	0.165
	P20	Surface (1–75 m)	19.040	3.138	0.398	6.298	1.453	0.065	2.620	0.188
Feb 2011 (2011–2001)	P12	Surface (1–65 m)	30.122	2.848	0.379	5.630	2.431	0.838	7.133	0.922
	P16	Surface (1–95 m)	16.230	1.286	0.202	5.728	1.726	0.161	4.439	1.643
	P20	Surface (1–77 m)	55.053	5.207	0.689	18.064	6.697	1.116	11.435	4.516
Jun 2011 (2011–2026)	P4	Surface (1–72 m)	29.791	2.635	0.127	10.619	2.663	0.720	5.836	5.234
	P12	Surface (1–90 m)	26.115	5.060	0.085	11.988	3.263	0.498	2.665	3.063
	P16	Surface (1–105 m)	22.088	4.044	0.104	11.390	2.195	0.181	2.612	1.569
	P20	Surface (1–70 m)	19.421	4.423	0.197	8.132	1.913	0.166	2.090	1.129
	P26	Surface (1–84 m)	29.376	7.239	0.184	10.532	4.406	0.232	3.723	2.663
		Flux at 100 m	0.765	0.474	0.036	0.059	0.0002	0.016	0.028	0.018
		% Flux	2.605	6.548	19.762	0.564	0.004	6.686	0.753	0.658
		Trap (150 m)	0.125	0.056	0.027	0.049	0.014	–	0.017	0.015
		% Flux	0.424	0.767	14.879	0.466	0.311	–	0.461	0.545
Feb 2012 (2012–01)	P4	Surface (1–38 m)	22.684	3.765	–	4.592	1.434	0.917	3.781	0.280
		Flux at 50 m	3.283	1.863	–	0.811	0.122	–	–	–
		% Flux	14.471	49.468	–	17.668	8.537	–	–	–
	P12	Surface (1–38 m)	11.003	1.425	0.116	5.606	1.894	0.017	1.915	0.500
		Flux at 100 m	0.046	0.020	0.000	0.014	0.005	0.000	0.000	0.000
		% Flux	0.415	1.381	0.000	0.254	0.249	0.000	0.000	0.000
	P26	Surface (1–38 m)	12.161	2.092	1.218	2.923	1.615	0.137	0.902	0.228
		Flux at 100 m	0.380	0.251	0.035	0.046	0.038	0.000	0.014	0.045
		% Flux	3.126	11.999	2.898	1.581	2.373	0.000	1.524	19.919
Jun 2012 (2012–12)	P4	Surface (1–103 m)	21.313	31.420	–	5.192	–	–	–	–
		Flux at 200 m	1.076	0.919	0.047	0.126	–	–	–	0.036
		% Flux	5.047	2.926	–	2.435	–	–	–	–
	P12	Surface (1–164 m)	27.677	5.967	–	22.445	6.552	–	–	–
		Flux at 200 m	0.051	0.047	–	0.075	0.010	–	0.025	–
		% Flux	0.185	0.787	–	0.335	0.156	–	–	–
	P16	Surface (1–66 m)	12.830	8.722	–	17.321	4.238	–	0.942	0.777
		Flux at 100 m	0.312	0.319	0.045	0.044	0.007	–	–	–
		% Flux	2.431	3.662	–	0.252	0.174	–	–	–
	P20	Surface (1–115 m)	18.344	33.038	–	13.892	–	–	13.090	3.538
		Flux at 100 m	0.016	0.016	0.004	–	0.002	–	0.005	0.001
		% Flux	0.088	0.049	–	–	–	–	0.036	0.033
	P26	Surface (1–60 m)	14.024	1.977	–	13.572	2.018	–	4.969	2.768
		Flux at 100 m	0.255	0.304	–	–	0.029	–	0.025	–
		% Flux	1.821	15.359	–	–	1.437	–	0.507	–
		Trap (100 m)	0.055	0.025	0.006	0.041	0.004	–	0.009	0.008
		% Flux	0.393	1.243	–	0.304	0.190	–	0.179	0.288

cruises, 4 ± 2 for the June cruises, and $5 \pm 3 \text{ cm s}^{-1}$ for the August cruise. These values agree well with the $\sim 10 \text{ cm s}^{-1}$ value reported by McNally (1981) and used by Charette et al. (1999). Given that the currents in the region generally flow west–east, and with no data at stations north and south of Line P, the north–south transport of ^{234}Th by advection

had to be assumed to be negligible. At stations P12, P16, and P20, the ^{234}Th gradient was measured between the adjacent stations. For stations P4 and P26 (at either end of Line P), the gradient of ^{234}Th was determined from the adjacent station assuming a linear change extended beyond the measured transect.

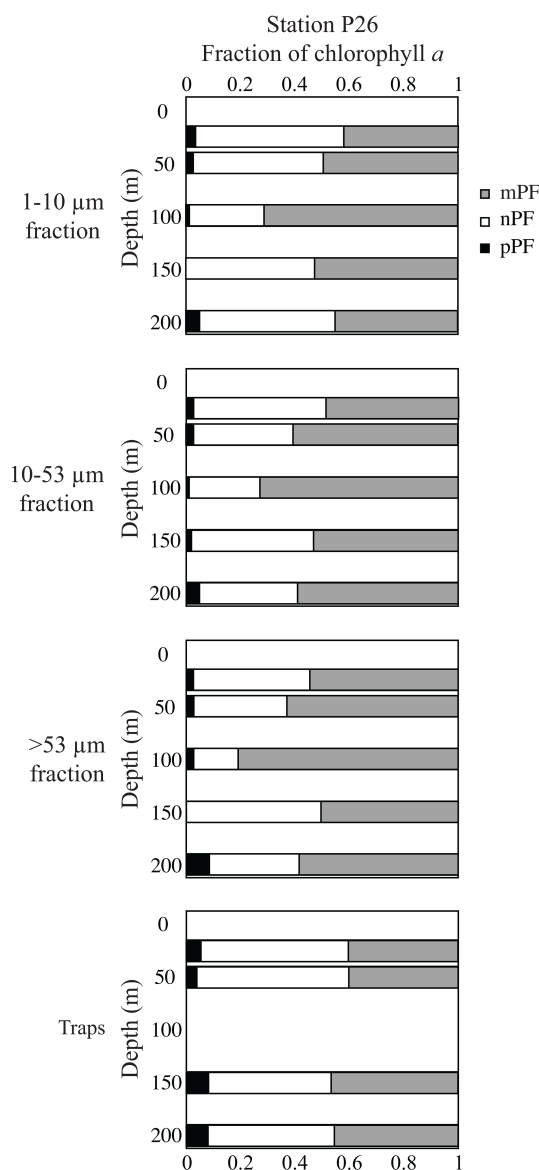


Figure 6. Pigment PFs for each phytoplankton size class plotted as a function of sample depth and particle size class at stations sampled on Line P in June 2011. Size-fractionated data are pump data. Sediment trap PFs are also included.

^{234}Th fluxes (P_{Th}) calculated using the 2-D model are within 5% of fluxes determined using a steady-state 1-D model that ignores advection (Fig. S4). This indicates that, under these assumptions, the vertical flux of ^{234}Th on sinking particles is the dominant transport term. Consistent with previous studies, ^{234}Th fluxes at all stations were higher during the August and June cruises than during the February cruises (Fig. 9a) (Charette et al., 1999). Also, ^{234}Th fluxes did not exhibit a consistent trend along Line P.

3.7 ^{234}Th -derived POC fluxes

The POC / ^{234}Th ratio in the $> 53 \mu\text{m}$ size class and P_{Th} for a given depth horizon were used to calculate POC fluxes (P_{POC}) (Fig. 9). In most cases, P_{POC} decreases with depth, although in some cases, the maximum P_{POC} in a given profile occurs at 50 or 100 m. P_{POC} fluxes at 100 m range from 0.65 to $7.95 \text{ mmol m}^{-2} \text{ d}^{-1}$; they are generally higher in summer than winter, and highest at station P4, consistent with previous studies at Line P (Charette et al., 1999; Wong et al., 1999; Timothy et al., 2013).

The ratio of P_{POC} flux to NPP, referred to as the ThE ratio, is an estimate of efficiency of the biological pump (Buesseler, 1998). ThE ratios determined using P_{POC} fluxes at the base of the photic zone (Table 3, Fig. 10) are similar to those reported by Charette et al. (1999), and are also in line with an annual average e ratio determined using average sediment trap POC fluxes (Wong et al., 1999) and annual average NPP (Harrison, 2002) (Fig. 10).

3.8 Sediment trap ^{234}Th and POC fluxes

The particle fluxes of both ^{234}Th and POC fluxes determined by the PITS traps (F_{Th} and F_{POC} , respectively) generally decrease with depth (Table 5). F_{Th} was higher in June 2012 than in June 2011, though there was no clear difference between the two cruises for F_{POC} . A comparison of the F_{Th} with the P_{Th} from corresponding stations and depths indicates that the F_{Th} is consistently higher than the P_{Th} , though usually not by more than a factor of 2. F_{POC} is also consistently higher than P_{POC} , though again not by more than a factor of 2 (Fig. 11a). The POC / ^{234}Th ratios of particles caught in sediment traps (Table 5) tend to be slightly higher (generally within a factor of 2) than the ratio of particles sampled by pumps at the corresponding station and depth.

3.9 ^{234}Th -derived and sediment trap pigment fluxes

Sinking fluxes of Chl a ($P_{\text{Chl } a}$) and indicator pigments (P_{Pigment}) were calculated from P_{Th} and the pigment / ^{234}Th ratio measured on $> 53 \mu\text{m}$ particles. Chl a and indicator pigment fluxes (Table 4, Fig. 12a–c) are generally highest at station P4 and decrease moving offshore. The highest indicator pigment fluxes were typically observed for microplankton pigments (FUCO and PER) whereas the lowest were observed for the picoplankton pigment ZEA (Table 4, Fig. 12a–c). It is important to note that the differences between fluxes of different pigments at a given station are determined by the pigment ratio on the $> 53 \mu\text{m}$ particles and are independent of P_{Th} .

Sediment trap pigment fluxes (F_{Pigment}) were typically lower than P_{Pigment} (Table 4, Fig. 11b). The maximum sediment trap fluxes of Chl a and most indicator pigments were determined at 50 m in June 2011 and at 30 m in June 2012 (Table 4). For both deployments the deepest fluxes were gen-

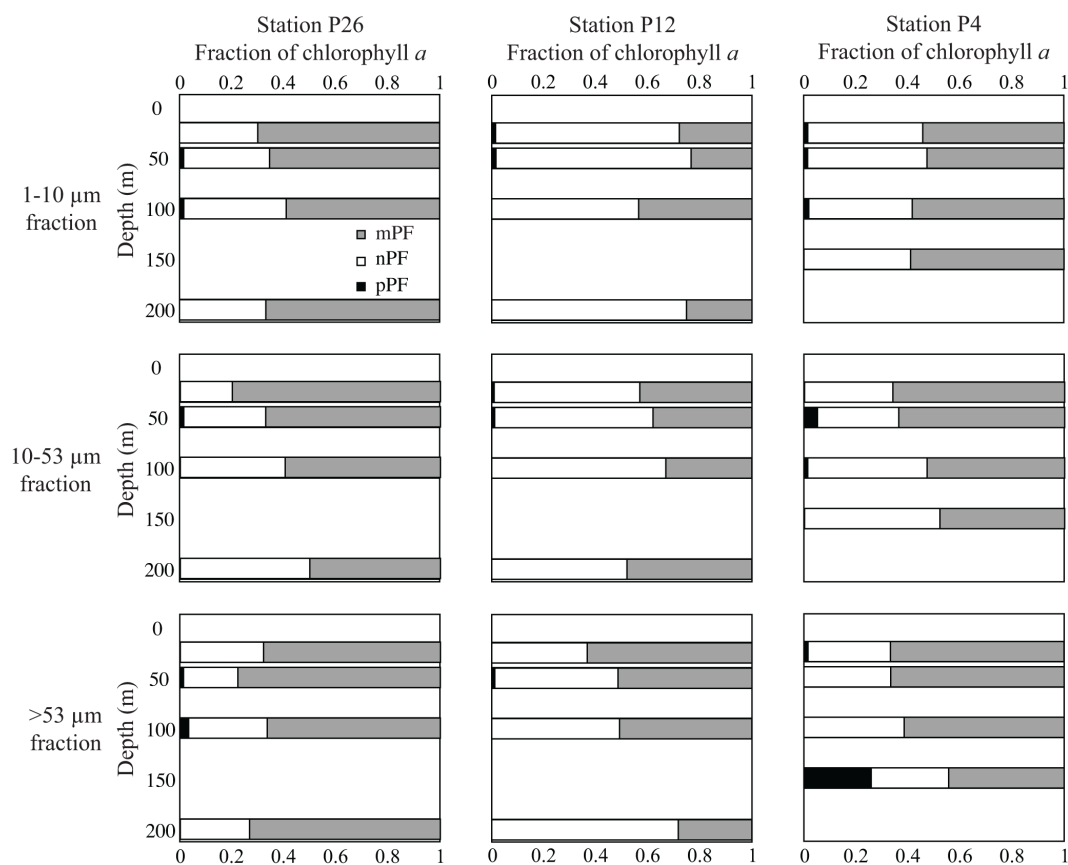


Figure 7. Pigment PFs for each phytoplankton size class plotted as a function of sample depth and particle size class at stations sampled on Line P in February 2012. Size-fractionated data are pump data.

Table 5. ^{234}Th and POC fluxes and POC / ^{234}Th ratios measured by the PITS traps.

Depth (m)	Days in situ	^{234}Th flux ($\text{dpm m}^{-2} \text{d}^{-1}$)	POC flux ($\text{mmol m}^{-2} \text{d}^{-1}$)	POC / ^{234}Th ratio ($\mu\text{mol dpm}^{-1}$)
Jun 2011 P26				
30	3.32	3192 ± 117	15.3 ± 0.4	4.8 ± 0.2
50	3.32	2909 ± 92	10.1 ± 0.3	3.5 ± 0.1
100	3.32	2256 ± 94	5.9 ± 0.2	2.6 ± 0.1
150	3.32	1928 ± 79	5.0 ± 0.2	2.6 ± 0.1
200	3.32	2281 ± 97	8.5 ± 0.3	3.7 ± 0.2
Jun 2012 P26				
30	2.82	3999 ± 206	14.7 ± 0.4	3.7 ± 0.2
50	2.82	5485 ± 290	13.5 ± 0.5	2.5 ± 0.2
100	2.82	3154 ± 192	6.5 ± 0.2	2.1 ± 0.1
150	2.82	2151 ± 135	5.5 ± 0.2	2.5 ± 0.2
200	2.82	3959 ± 129	5.0 ± 0.2	1.3 ± 0.1

erally the lowest, presumably due to the progressive degradation of sinking phytoplankton and resulting loss of pigments. Chl *a* and indicator pigment fluxes were generally higher in June 2011 than in June 2012, which is the opposite of the trend observed for F_{Th} .

Pigment PFs determined for material captured by the PITS traps do not vary greatly with depth, suggesting that the quality of material sinking to depth is similar to that in the surface water, despite the general decrease of material (Figs. 6 and 8). Microplankton PFs are higher for trap samples than for

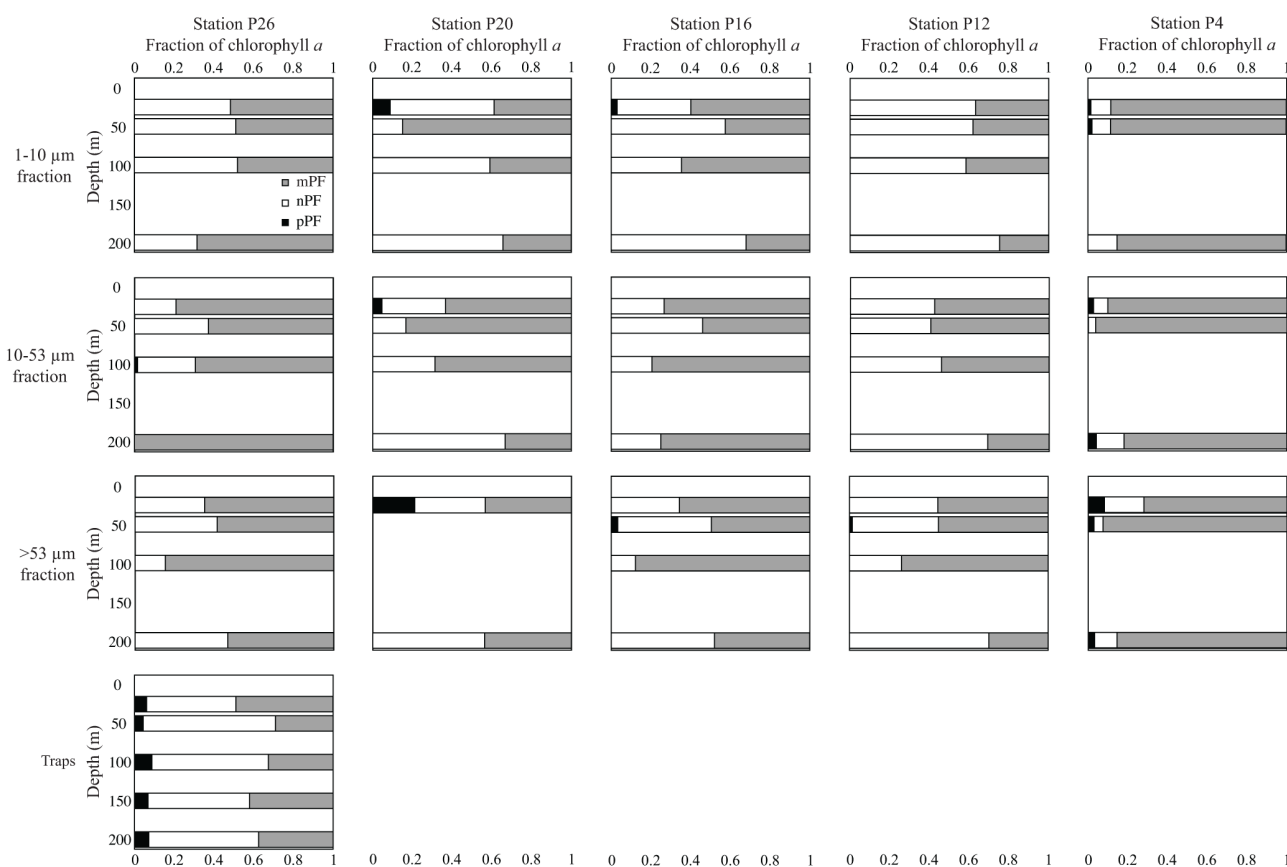


Figure 8. Pigment PFs for each phytoplankton size class plotted as a function of sample depth and particle size class at stations sampled on Line P in June 2012. Size-fractionated data are pump data. Sediment trap PFs are also included where available.

bottle samples but not as high as for pump samples, while nPFs and pPFs are higher for trap samples than for pump samples but lower than for bottle samples.

4 Discussion

The results presented in this study build on previous investigations of export production in the northeast Pacific by providing estimates of the relative contributions of different phytoplankton size classes to particle export. A comparison of indicator pigment standing stocks determined from small-volume samples and P_{Pigment} fluxes suggests that while nanoplankton represented the bulk of phytoplankton biomass ($68 \pm 24\%$ of pigment standing stocks, averaged for all stations and cruises), microplankton dominated the flux of pigmented material ($69 \pm 19\%$ on average) (Table 4, Fig. 12). Sediment trap pigment fluxes indicate a lower, but still substantial, relative contribution of microplankton to export, with microplankton pigments making up 47 and 33% of the total sediment trap indicator pigment flux in June 2011 and June 2012, respectively, as compared to 81 and 85% of total P_{Pigment} fluxes. Though nano- and picoplankton did not form the majority of the algal aggregate flux, their $29 \pm 19\%$ con-

tribution is significant and similar to contributions reported by Lomas and Moran (2011) for cyanobacteria and nano-eukaryotes in the Sargasso Sea.

Indicator pigment loss rates determined from both P_{Pigment} fluxes and sediment trap pigment fluxes imply that microplankton are exported more efficiently than nano- or picoplankton (Table 4, Fig. 12d–f). Loss rates of pigments, estimated as the ratio of P_{Pigment} fluxes to pigment standing stocks, averaged (for all cruises) $8 \pm 12\%$ for microplankton pigments, $1 \pm 2\%$ for nanoplankton pigments and $0.6 \pm 1\%$ for picoplankton pigments. These results suggest that export of large cells by direct sinking of algal aggregates is more efficient than the export of small cells by the same pathway. Sediment trap loss rates for microplankton were also higher than those for nano- and picoplankton, further indicating preferential export of microplankton. Even though differences between bottle and pump samples may exaggerate the extent to which large cells dominate export, sediment trap loss rates support and confirm the preferential export of large cells by algal aggregation.

In contrast to the trends observed for pigment fluxes and loss rates, the low variability of pump indicator pigment PFs with depth (Figs. 6–8) does not appear to indicate preferential

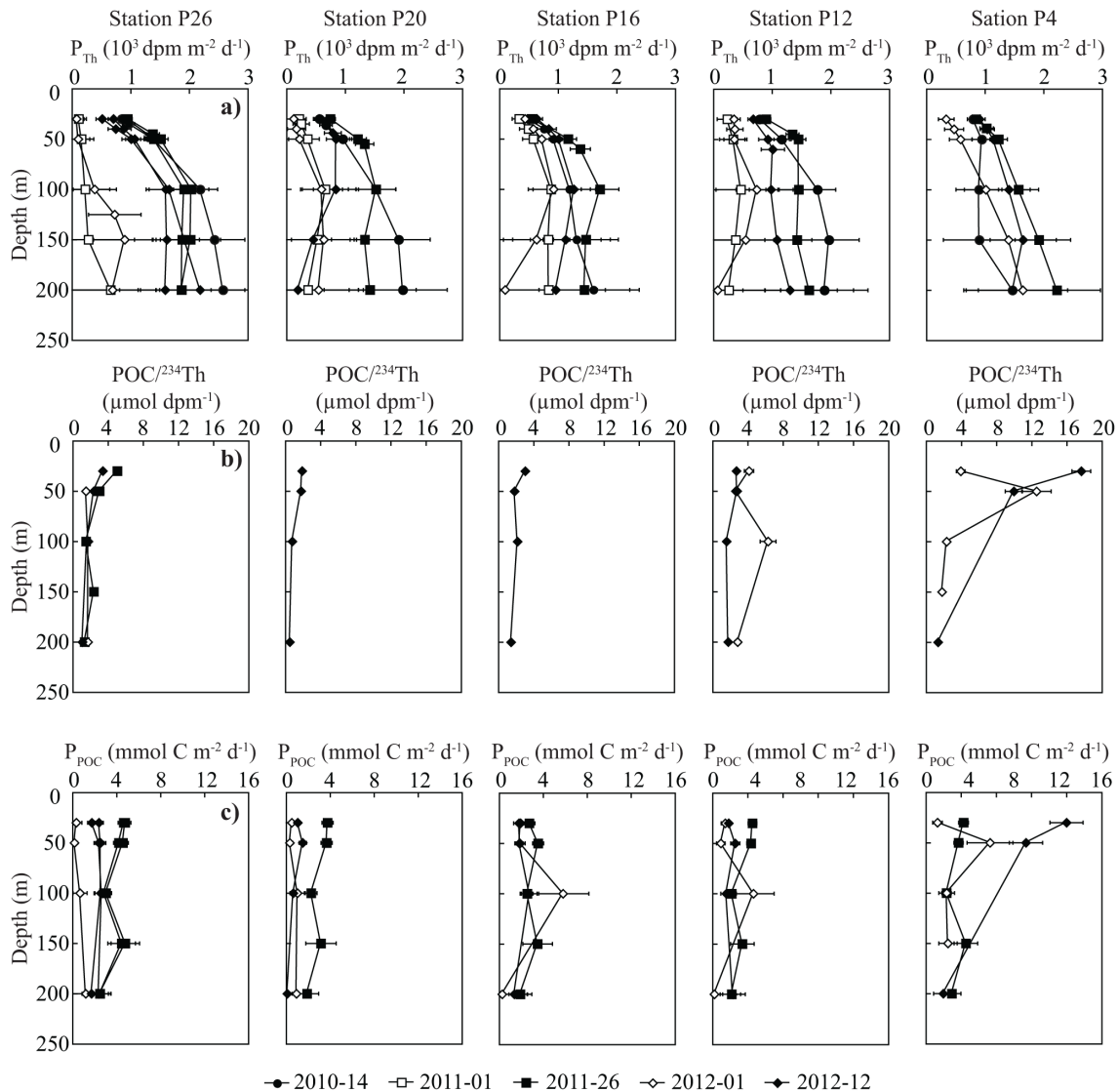


Figure 9. Depth profiles of (a) ^{234}Th fluxes (P_{Th}) determined using the 2-D model, (b) POC/ ^{234}Th ratios on $> 53 \mu m$ particles, and (c) ^{234}Th -derived POC fluxes (P_{POC}) at stations on Line P during the five cruises in this study.

export of microplankton. Furthermore, the presence of nano- and picoplankton pigments in the $> 53 \mu m$ size fraction and in samples below the mixed layer suggests that nano- and picoplankton are incorporated into aggregates and that some of these aggregates are exported from the surface ocean. If large cells were preferentially exported, microplankton pigments would be expected to make up a larger percentage of total pigments in samples below the mixed layer than in samples from the mixed layer, but this is not observed in the results of this study. It is possible that some of this discrepancy can be attributed to differences between bottle and pump samples. Because cells $< 1 \mu m$ in size can pass through the $1 \mu m$ Nitex screens used in the pumps, the sum of the pump size fractions does not accurately reflect the community composition in the euphotic zone, and may miss a change in indicator

pigment PFs with depth. In addition, the under-sampling of large cells by Niskin bottles may lead to an underestimate of microplankton standing stocks, and thus an overestimate of microplankton loss rates.

These pigment fluxes are likely lower estimates of the total contribution of each phytoplankton group to particle export. The use of indicator pigments as tracers of phytoplankton export only accounts for the direct sinking of healthy, ungrazed cells, because grazing degrades the indicator pigments to an analytically undetectable form (Head and Harris, 1992; Strom et al., 1998; Thibault et al., 1999). Indirect export (via grazing) is thought to be an important pathway for picoplankton export in the HNLC equatorial Pacific (Richardson et al., 2004; Stukel and Landry, 2010). Given that grazing has been shown to control the biomass of small phytoplankton in the

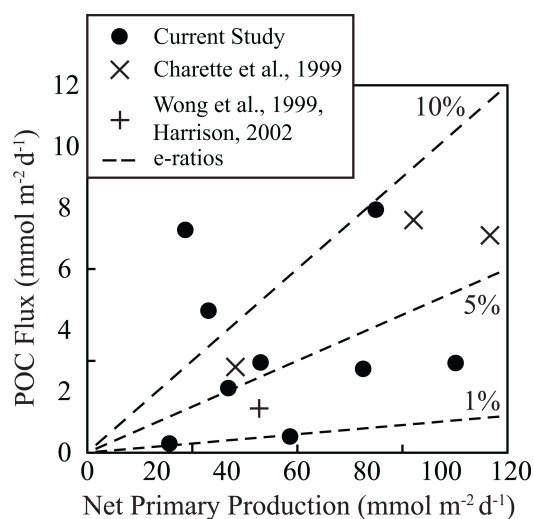


Figure 10. Net primary production (NPP) plotted against ^{234}Th -derived POC fluxes (P_{POC}) for stations along Line P in this study. The slopes of the dashed lines represent ThE ratios. For reference, NPP and P_{POC} values determined by Charette et al. (1999) for winter, spring, and summer are included, along with annual average NPP and sediment trap POC fluxes (at 200 m) reported in Harrison (2002) and Wong et al. (1999), respectively.

northeast Pacific (Landry et al., 1993; Harrison et al., 1999; Rivkin et al., 1999), indirect export may also be a significant pathway for small cell export in this region. Because this pathway is not accounted for by the methodology employed in this study, the results presented here may underestimate the export of small phytoplankton, which may be less likely to sink directly. It is also possible that grazing contributes further to enhanced export of large phytoplankton as suggested by traditional models of the biological pump (e.g., Michaels and Silver 1988).

Although grazing and fecal pellet export were not directly measured in this study, a comparison of sediment trap and pump measurements of Chl *a*, indicator pigments, and POC suggests that zooplankton fecal pellets may be an important component of POC export at OSP, at least in spring (Fig. 11). While F_{POC} fluxes are higher than the corresponding P_{POC} fluxes, F_{Pigment} fluxes are lower than P_{Pigment} fluxes, indicating that the material captured by the sediment traps is enriched in carbon and depleted in Chl *a* and indicator pigments relative to that sampled by the pumps. Because the trap brine was not poisoned, zooplankton grazing and cell degradation in the trap tube may also have contributed to some loss of pigments over the ~ 3 -day deployment of the PITS traps. However, the collection of carbon-rich and pigment-depleted fecal pellets by the traps but not by the pumps, which do not quantitatively sample fecal pellets (Lomas and Moran, 2011), could also explain these observations. This latter explanation is consistent with the results presented in Thibault

et al. (1999), which indicate that fecal pellet export is 3 to 6 times greater than algal aggregate export at Line P.

5 Conclusions

New estimates of phytoplankton indicator pigment loss rates calculated from both ^{234}Th -derived and sediment trap pigment fluxes suggest that large cells are preferentially exported at Line P. Specifically, microplankton pigments on average made up $69 \pm 19\%$ of the total pigment flux, but only $32 \pm 24\%$ of pigment standing stocks (determined from small-volume samples), whereas nano- and picoplankton pigments on average formed $31 \pm 19\%$ of pigment flux in spite of representing $68 \pm 24\%$ of the standing stocks. These results are consistent with traditional food web models (Michaels and Silver, 1988; Legendre and Le Fèvre, 1995) that suggest nano- and picoplankton are underrepresented in particle flux relative to their contribution to phytoplankton biomass; they also lend support to the conclusions of Choi et al. (2014). However, the methods employed in this study do not quantitatively account for export via zooplankton fecal pellets, which could be significant for small phytoplankton as they are controlled by grazing in this region (Landry et al., 1993; Harrison et al., 1999; Rivkin et al., 1999; Thibault et al., 1999). Furthermore, the determination of pigment loss rates also required a comparison between small- and large-volume samples, and the inherent differences of these sampling techniques likely led to an overestimation of the microplankton contribution to algal aggregate export. Therefore, it is possible that all size classes of phytoplankton contribute to POC export in approximate proportion to their contribution to NPP as predicted by Richardson and Jackson (2007).

This study, conducted in a subarctic HNLC region, contributes to the ongoing discussion of small cell export that has largely focused on tropical and subtropical regions (Richardson et al., 2004, 2006; Richardson and Jackson, 2007; Stukel and Landry, 2010; Lomas and Moran, 2011). In particular, these results suggest that nano- and picoplankton may contribute significantly to POC export in this subarctic HNLC region, even if they are not as efficiently exported as larger microplankton. If large phytoplankton drive more efficient POC export in the northeast Pacific as suggested by this study, it could have important implications for understanding the biological pump. It has been proposed that decreasing winter mixed layer depths (Freeland et al., 1997; Freeland, 2013) and variations of macronutrient concentrations linked to shifts in climate regime (Pena and Varela, 2007) in the northeast Pacific could lead to shifts in the phytoplankton community composition. This study suggests that such changes in phytoplankton community composition could significantly affect the efficiency of the biological pump, and in turn, the cycling of carbon. While the results indicate that shifts in community composition favoring larger phyto-

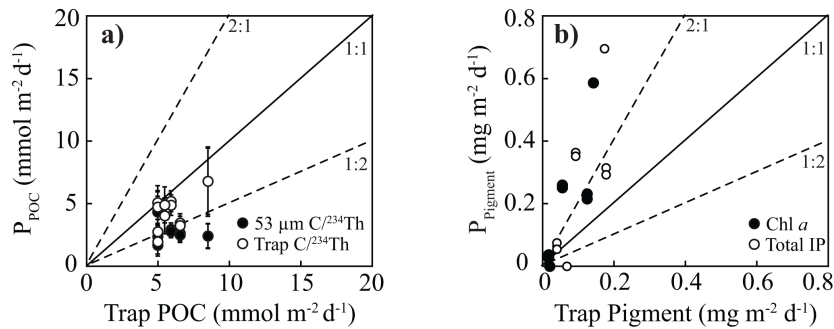


Figure 11. (a) Comparison of sediment trap POC fluxes and ²³⁴Th-derived POC fluxes, and (b) a comparison of sediment trap Chl *a* and total indicator pigment fluxes and ²³⁴Th-derived pigments fluxes at OSP during June 2011 and June 2012.

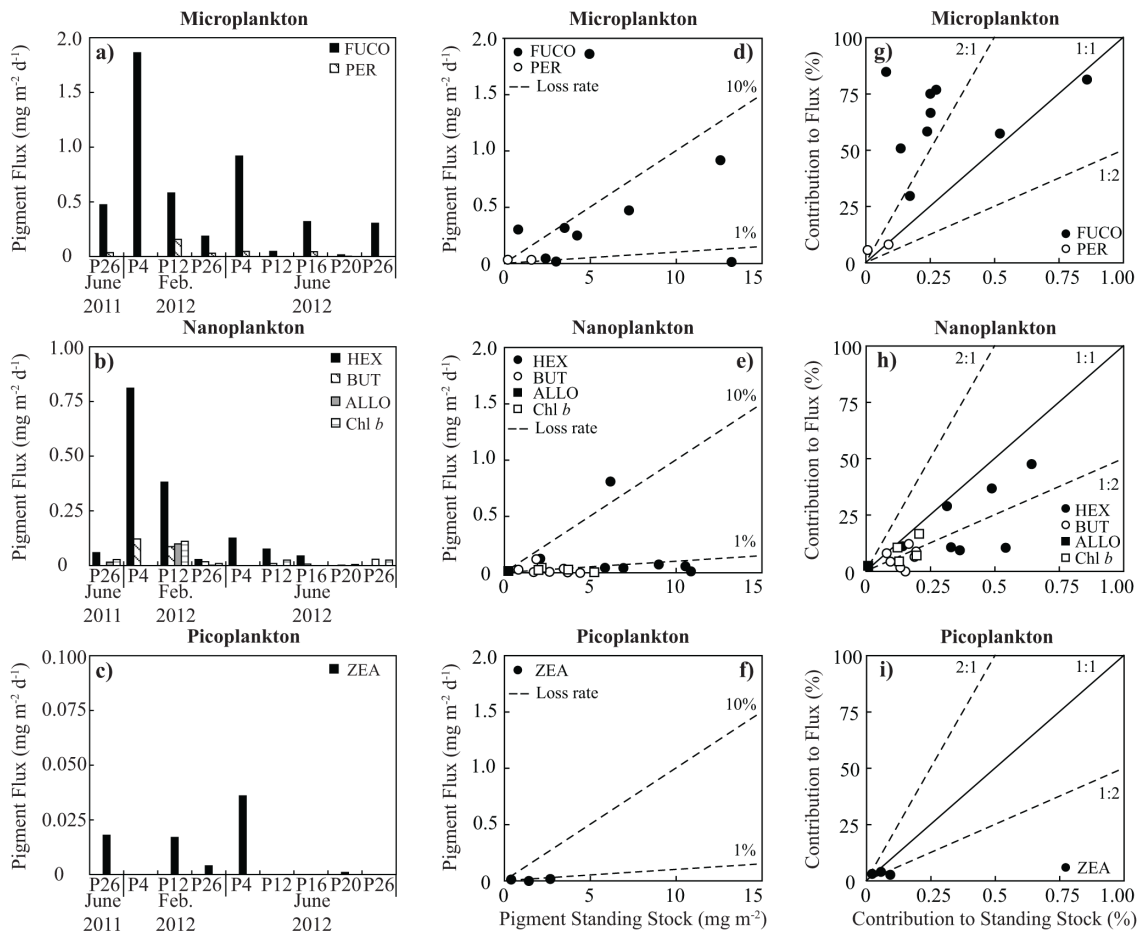


Figure 12. (a–c) ²³⁴Th-derived indicator pigment fluxes determined using the pigment / ²³⁴Th ratio on > 53 μm particles plotted for micro-, nano-, and picoplankton pigments. (d–f) Indicator pigment standing stocks plotted against indicator pigment fluxes for micro-, nano-, and picoplankton pigments. The slopes of the dashed lines indicate pigment loss rates. (g–i) The contribution to total pigment standing stocks plotted against the contribution to total pigment flux for micro-, nano-, and picoplankton pigments. Data points above the 1 : 1 line indicate preferential export by direct sinking, and points below the 1 : 1 line indicate disproportionately low export by direct sinking relative to biomass contributions.

plankton could lead to more efficient particle export, they do not indicate that shifts favoring smaller phytoplankton would lead to a shutdown of POC export as suggested by some pre-

vious studies (e.g., Michaels and Silver, 1988), but merely that the export of POC could be less efficient.

The Supplement related to this article is available online at doi:10.5194/bg-12-3429-2015-supplement.

Acknowledgements. We thank the captain and crew of the CCGS *John P. Tully*, Marie Robert and the Line P Program collaborators, Doug Bell for at-sea sampling and laboratory assistance, and Matthew Baumann for his laboratory assistance. This research was supported by the National Science Foundation grants OCE 0926311 to S. B. Moran, OCE 0927559 to M. W. Lomas, and OCE 0926348 to G. M. Stewart.

Edited by: K. Suzuki

References

- Amacher, J., Neuer, S., Anderson, I., and Massana, R.: Molecular approach to determine contributions of the protist community to particle flux, *Deep-Sea Res. Part Oceanogr. Res. Pap.*, 56, 2206–2215, 2009.
- Baumann, M. S., Moran, S. B., Lomas, M. W., Kelly, R. P., and Bell, D. W.: Seasonal decoupling of particulate organic carbon export and net primary production in relation to sea-ice at the shelf break of the eastern Bering Sea: Implications for off-shelf carbon export, *J. Geophys. Res. Oceans*, 118, 5504–5522, 2013.
- Benitez-Nelson, C. R., Buesseler, K. O., Van der Loeff, M. R., Andrews, J., Ball, L., Crossin, G., and Charette, M. A.: Testing a new small-volume technique for determining ^{234}Th in seawater, *J. Radioanal. Nucl. Chem.*, 248, 795–799, 2001.
- Bograd, S. J., Thomson, R. E., Rabinovich, A. B., and LeBlond, P. H.: Near-surface circulation of the northeast Pacific Ocean derived from WOCE-SVP satellite-tracked drifters, *Deep-Sea Res. Part II Top. Stud. Oceanogr.*, 46, 2371–2403, 1999.
- Boyd, P. and Harrison, P. J.: Phytoplankton dynamics in the (NE) subarctic Pacific, *Deep-Sea Res. Part II Top. Stud. Oceanogr.*, 46, 2405–2432, 1999.
- Boyd, P. W. and Newton, P. P.: Does planktonic community structure determine downward particulate organic carbon flux in different oceanic provinces?, *Deep-Sea Res. Part Oceanogr. Res. Pap.*, 46, 63–91, 1999.
- Brew, H. S., Moran, S. B., Lomas, M. W., and Burd, A. B.: Plankton community composition, organic carbon and thorium-234 particle size distributions, and particle export in the Sargasso Sea, *J. Mar. Res.*, 67, 845–868, 2009.
- Buesseler, K. O.: The decoupling of production and particulate export in the surface ocean, *Glob. Biogeochem. Cy.*, 12, 297–310, 1998.
- Buesseler, K. O., Benitez-Nelson, C., Rutgers van der Loeff, M., Andrews, J., Ball, L., Crossin, G., and Charette, M. A.: An intercomparison of small-and large-volume techniques for thorium-234 in seawater, *Mar. Chem.*, 74, 15–28, 2001.
- Burd, A. B., Jackson, G. A., and Moran, S. B.: The role of the particle size spectrum in estimating POC fluxes from disequilibrium, *Deep-Sea Res. Part Oceanogr. Res. Pap.*, 54, 897–918, 2007.
- Charette, M. A., Moran, S. B., and Bishop, J. K. B.: ^{234}Th as a tracer of particulate organic carbon export in the subarctic northeast Pacific Ocean, *Deep-Sea Res. Part II Top. Stud. Oceanogr.*, 46, 2833–2861, 1999.
- Chen, J. H., Lawrence Edwards, R., and Wasserburg, G. J.: ^{238}U , ^{234}U and ^{232}Th in seawater, *Earth Planet. Sci. Lett.*, 80, 241–251, 1986.
- Choi, H. Y., Stewart, G. M., Lomas, M. W., Kelly, R. P., and Moran, S. B.: Linking the distribution of ^{210}Po and ^{210}Pb with plankton community along Line P, Northeast Subarctic Pacific, *J. Environ. Radioact.*, 138, 390–401, 2014.
- Coale, K. H. and Bruland, K. W.: ^{234}Th : ^{238}U disequilibria within the California Current, *Limnol. Ocean.*, 30, 22–33, 1985.
- Emerson, S.: Annual net community production and the biological carbon flux in the ocean, *Glob. Biogeochem. Cy.*, 28, 14–28, 2014.
- Freeland, H., Denman, K., Wong, C. S., Whitney, F., and Jacques, R.: Evidence of change in the winter mixed layer in the Northeast Pacific Ocean, *Deep-Sea Res. Part Oceanogr. Res. Pap.*, 44, 2117–2129, 1997.
- Freeland, H. J.: Evidence of Change in the Winter Mixed Layer in the Northeast Pacific Ocean: A Problem Revisited, *Atmos.-Oc.*, 51, 126–133, 2013.
- Gardner, W. D.: Incomplete extraction of rapidly settling particles from water samplers, *Limnol. Ocean.*, 22, 764–768, 1977.
- Gundersen, K., Orcutt, K. M., Purdie, D. A., Michaels, A. F., and Knap, A. H.: Particulate organic carbon mass distribution at the Bermuda Atlantic Time-series Study (BATS) site, *Deep-Sea Res. Part II Top. Stud. Oceanogr.*, 48, 1697–1718, 2001.
- Harrison, P. J.: SERIES (subarctic ecosystem response to iron enrichment study): A Canadian–Japanese contribution to our understanding of the iron–ocean–climate connection, *Deep-Sea Res. Part II Top. Stud. Oceanogr.*, 53, 2006–2011, 2006.
- Harrison, P. J., Boyda, P. W., Varela, D. E., Takeda, S., Shiimoto, A., and Odate, T.: Comparison of factors controlling phytoplankton productivity in the (NE) and (NW) subarctic Pacific gyres, *Prog. Oceanogr.*, 43, 205–234, 1999.
- Head, E. J. H. and Harris, L. R.: Chlorophyll and carotenoid transformation and destruction by *Calanus* spp. grazing on diatoms, *Mar. Ecol.-Prog. Ser.*, 86, 229–229, 1992.
- Hooker, S. B., Van Heukelem, L., Thomas, C. S., Claustre, H., Ras, J., Barlow, R., Sessions, H., Schlüter, L., Perl, J., and Trees, C.: Second SeaWiFS HPLC Analysis Round-robin Experiment (SeaHARRE-2), National Aeronautics and Space Administration, Goddard Space Flight Center, 2005.
- Irwin, A. J., Finkel, Z. V., Schofield, O. M. E., and Falkowski, P. G.: Scaling-up from nutrient physiology to the size-structure of phytoplankton communities, *J. Plankton Res.*, 28, 459–471, 2006.
- Knap, A. H., Michaels, A. F., Steinberg, D. K., Bahr, F., Bates, N. R., Bell, S., Countway, P., Close, A. R., Doyle, A. P., and Dow, R. L.: BATS Methods manual, version 4, 1997.
- Landry, M. R., Monger, B. C., and Selph, K. E.: Time-dependency of microzooplankton grazing and phytoplankton growth in the subarctic Pacific, *Prog. Oceanogr.*, 32, 205–222, 1993.
- Legendre, L. and Le Fèvre, J.: Microbial food webs and the export of biogenic carbon in oceans, *Aquat. Microb. Ecol.*, 9, 69–77, 1995.
- Liu, Z., Stewart, G., Kirk Cochran, J., Lee, C., Armstrong, R. A., Hirschberg, D. J., Gasser, B., and Miquel, J.-C.: Why do POC concentrations measured using Niskin bottle collections sometimes differ from those using in-situ pumps?, *Deep-Sea Res. Part Oceanogr. Res. Pap.*, 52, 1324–1344, 2005.

- Liu, Z., Cochran, J. K., Lee, C., Gasser, B., Miquel, J. C., and Wakeham, S. G.: Further investigations on why (POC) concentrations differ in samples collected by Niskin bottle and in situ pump, *Deep-Sea Res. Part II Top. Stud. Oceanogr.*, 56, 1558–1567, 2009.
- Lomas, M. W. and Moran, S. B.: Evidence for aggregation and export of cyanobacteria and nano-eukaryotes from the Sargasso Sea euphotic zone, *Biogeosciences*, 8, 203–216, doi:10.5194/bg-8-203-2011, 2011.
- Lomas, M. W., Moran, S. B., Casey, J. R., Bell, D. W., Tiahlo, M., Whitefield, J., Kelly, R. P., Mathis, J. T., and Cokelet, E. D.: Spatial and seasonal variability of primary production on the Eastern Bering Sea shelf, *Deep-Sea Res. Part II Top. Stud. Oceanogr.*, 65–70, 126–140, 2012.
- Marchetti, A., Sherry, N. D., Kiyosawa, H., Tsuda, A., and Harrison, P. J.: Phytoplankton processes during a mesoscale iron enrichment in the NE subarctic Pacific: Part I – biomass and assemblage, *Deep-Sea Res. Part II Top. Stud. Oceanogr.*, 53, 2095–2113, 2006.
- McNally, G. J.: Satellite tracked drift buoy observations of the near surface flow in the eastern mid latitude North Pacific, *J. Geophys. Res. Oceans* 1978–2012, 86, 8022–8030, 1981.
- Michaels, A. F. and Silver, M. W.: Primary production, sinking fluxes and the microbial food web, *Deep-Sea Res. Part Oceanogr. Res. Pap.*, 35, 473–490, 1988.
- Moran, S. B., Charette, M. A., Pike, S. M., and Wicklund, C. A.: Differences in seawater particulate organic carbon concentration in samples collected using small- and large-volume methods: the importance of DOC adsorption to the filter blank, *Mar. Chem.*, 67, 33–42, 1999.
- Moran, S. B., Weinstein, S. E., Edmonds, H. N., Smith, J. N., Kelly, R. P., Pilson, M. E. Q., and Harrison, W. G.: Does $^{234}\text{Th}/^{238}\text{U}$ disequilibrium provide an accurate record of the export flux of particulate organic carbon from the upper ocean?, *Limnol. Oceanogr.*, 48, 1018–1029, 2003.
- Morán, X. A. G., López-Urrutia, Á., Calvo Díaz, A., and Li, W. K.: Increasing importance of small phytoplankton in a warmer ocean, *Glob. Change Biol.*, 16, 1137–1144, 2010.
- Muggli, D. L., Lecourt, M., and Harrison, P. J.: Effects of iron and nitrogen source on the sinking rate, physiology and metal composition of an oceanic diatom from the subarctic Pacific, *Oceanogr. Lit. Rev.*, 43, 215–227, 1996.
- Pena, M. A. and Varela, D. E.: Seasonal and interannual variability in phytoplankton and nutrient dynamics along Line P in the NE subarctic Pacific, *Prog. Oceanogr.*, 75, 200–222, 2007.
- Polovina, J. J., Howell, E. A., and Abecassis, M.: Ocean's least productive waters are expanding, *Geophys. Res. Lett.*, 35, L03618, doi:10.1029/2007GL031745, 2008.
- Richardson, T. L. and Jackson, G. A.: Small phytoplankton and carbon export from the surface ocean, *Science*, 315, 838–840, 2007.
- Richardson, T. L., Jackson, G. A., Ducklow, H. W., and Roman, M. R.: Carbon fluxes through food webs of the eastern equatorial Pacific: an inverse approach, *Deep-Sea Res. Part Oceanogr. Res. Pap.*, 51, 1245–1274, 2004.
- Richardson, T. L., Jackson, G. A., Ducklow, H. W., and Roman, M. R.: Spatial and seasonal patterns of carbon cycling through planktonic food webs of the Arabian Sea determined by inverse analysis, *US JGOFS Synth. Model. Proj. Phase III US JGOFS Synth. Model. Proj. Phase III*, 53, 555–575, 2006.
- Rivkin, R. B., Putland, J. N., Robin Anderson, M., and Deibel, D.: Microzooplankton bacterivory and herbivory in the NE subarctic Pacific, *Deep-Sea Res. Part II Top. Stud. Oceanogr.*, 46, 2579–2618, 1999.
- Speicher, E. A., Moran, S. B., Burd, A. B., Delfanti, R., Kaberi, H., Kelly, R. P., Papucci, C., Smith, J. N., Stavrakakis, S., and Torricelli, L.: Particulate organic carbon export fluxes and size-fractionated POC/Th ratios in the Ligurian, Tyrrhenian and Aegean Seas, *Deep-Sea Res. Part Oceanogr. Res. Pap.*, 53, 1810–1830, 2006.
- Strom, S., Morello, T., and Bright, K.: Protozoan size influences algal pigment degradation during grazing, *Mar. Ecol. Prog. Ser. Halstenbek*, 164, 189–197, 1998.
- Stukel, M. R. and Landry, M. R.: Contribution of picophytoplankton to carbon export in the equatorial Pacific: A reassessment of food web flux inferences from inverse models, *Limnol. Oceanogr.*, 55, 2669–2685, 2010.
- Stukel, M. R., Décima, M., Selph, K. E., Taniguchi, D. A., and Landry, M. R.: The role of *Synechococcus* in vertical flux in the Costa Rica upwelling dome, *Prog. Oceanogr.*, 112, 49–59, 2013.
- Thibault, D., Roy, S., Wong, C. S., and Bishop, J. K.: The downward flux of biogenic material in the NE subarctic Pacific: importance of algal sinking and mesozooplankton herbivory, *Deep-Sea Res. Part II Top. Stud. Oceanogr.*, 46, 2669–2697, 1999.
- Timothy, D. A., Wong, C. S., Barwell-Clarke, J. E., Page, J. S., White, L. A., and Macdonald, R. W.: Climatology of sediment flux and composition in the subarctic Northeast Pacific Ocean with biogeochemical implications, *Prog. Oceanogr.*, 116, 95–129, 2013.
- Van der Loeff, M. R., Sarin, M. M., Baskaran, M., Benitez-Nelson, C., Buesseler, K. O., Charette, M., Dai, M., Gustafsson, Ö., Masque, P., and Morris, P. J.: A review of present techniques and methodological advances in analyzing ^{234}Th in aquatic systems, *Mar. Chem.*, 100, 190–212, 2006.
- Wong, C. S., Whitney, F. A., Crawford, D. W., Iseki, K., Matear, R. J., Johnson, W. K., Page, J. S., and Timothy, D.: Seasonal and interannual variability in particle fluxes of carbon, nitrogen and silicon from time series of sediment traps at Ocean Station P, 1982–1993: Relationship to changes in subarctic primary productivity, *Deep-Sea Res. Part II Top. Stud. Oceanogr.*, 46, 2735–2760, 1999.